Numerical Analysis of a Keller-Segel-Flow Model for Tumor Cell Migration

A. Fernandes[1], J.A. Ferreira[1], and L. Pinto[1]
[1]University of Coimbra, CMUC, Department of Mathematics, Coimbra, Portugal
augusto98@outlook.com, ferreira@mat.uc.pt, luisp@mat.uc.pt

November 25, 2024

Abstract

Understanding the mechanisms underlying tumor metastasis is critical for designing effective anti-tumor therapies. This article focuses on the modeling and numerical analysis of cell migration by chemical signals and interstitial flow, two crucial factors in tumor metastasis. We consider a nonlinear Keller-Segel model that includes an elliptic equation based on Darcy's law for fluid flow. We propose a fully discrete method that combines an implicit-explicit method in time with a finite difference method in space. We establish the method's second-order superconvergence in space in a discrete H^1-norm, optimal first-order convergence in time in a discrete L^2-norm, and local nonlinear stability. Numerical simulations confirm the sharpness of the error analysis. We also look into the model's ability to reproduce laboratory experiments on the effects of flow and chemotaxis on tumor cell migration.

Keywords: Tumour cell migration; Keller-Segel-Flow model; Numerical analysis; Optimal error estimates; Numerical simulation.

1 Introduction

Let us consider $\Omega = (0,1)^2$ and define in $\Omega \times (0,T]$ the nonlinear elliptic-parabolic system

$$\begin{cases} \dfrac{\partial c_b}{\partial t} + \nabla \cdot (\phi(\nabla c_c, c_c, \nabla p) c_b) = \nabla \cdot (D_b(c_b, c_c) \nabla c_b) + f(c_b, c_c), & (1) \\ \dfrac{\partial c_c}{\partial t} + \nabla \cdot (\psi(\nabla p) c_c) = \nabla \cdot (D_c(c_b, c_c) \nabla c_c) + g(c_b, c_c), & (2) \\ -\nabla \cdot (D_p(c_b, c_c) \nabla p) = q(c_b, c_c, p), & (3) \end{cases}$$

with initial conditions

$$c_b(x,y,0) = c_{b,0}(x,y), \quad c_c(x,y,0) = c_{c,0}(x,y), \quad p(x,y,0) = p_0(x,y), \quad (x,y) \in \Omega, \qquad (4)$$

and the Dirichlet boundary conditions

$$\begin{cases} c_b(x,y,t) = c_c(x,y,t) = 0, & \partial\Omega \times (0,T], \\ p(x,y,t) = p_1(x,y,t), & \Gamma_1 \times (0,T], \\ p(x,y,t) = p_2(x,y,t), & \Gamma_2 \times (0,T], \end{cases} \qquad (5)$$

with $\overline{\Gamma}_1 \cup \overline{\Gamma}_2 = \partial\Omega$ and $\Gamma_1 \cap \Gamma_2 = \emptyset$.

In (1)-(3), $q : \mathbb{R}^3 \to \mathbb{R}$, $f, g : \mathbb{R}^2 \to \mathbb{R}$, D_b, D_c, and D_p are diagonal matrices depending on c_b and c_c

$$D_b(c_b, c_c) = \begin{bmatrix} D_{b,11}(c_b, c_c) & 0 \\ 0 & D_{b,22}(c_b, c_c) \end{bmatrix}, \quad D_{b,ii} : \mathbb{R}^2 \to \mathbb{R},\ i = 1, 2, \tag{6}$$

with analogous meaning for D_c and D_p, and

$$\phi(\nabla c_c, c_c, \nabla p) = \begin{bmatrix} \phi_1(\frac{\partial c_c}{\partial x}, c_c, \frac{\partial p}{\partial x}) \\ \phi_2(\frac{\partial c_c}{\partial y}, c_c, \frac{\partial p}{\partial y}) \end{bmatrix}, \quad \phi_i : \mathbb{R}^3 \to \mathbb{R},\ i = 1, 2, \tag{7}$$

$$\psi(\nabla p) = \begin{bmatrix} \psi_1(\frac{\partial p}{\partial x}) \\ \psi_2(\frac{\partial p}{\partial y}) \end{bmatrix}, \quad \psi_i : \mathbb{R}^2 \to \mathbb{R},\ i = 1, 2. \tag{8}$$

The seminal 1970s Keller-Segel model is a particular case of the generic equations (1)-(2). This model describes how cell density c_b evolves under the influence of chemical signal concentration c_c, a process called autologous chemotaxis. Over the years, researchers have adapted the Keller-Segel model to describe various biological processes, and we refer to [1] for a comprehensive overview of these variations.

Our focus is on biological processes where convective flow plays an important role. Specifically, we investigate the migration of tumor cells under interstitial flow. The interstitial flow is the fluid motion through the porous extracellular matrix (ECM) driven by the pressure gradient between surrounding blood and lymphatic capillaries. In this context, Darcy's equation (3) governs the pressure field p, where D_p represents the ECM's permeability and q describes fluid exchanges between capillaries and the ECM. The function $\phi(\nabla c_c, c_c, \nabla p)$ in equation (1) describes the cells' sensitivity to interstitial flow and chemical concentration, while $\psi(\nabla p)$ in equation (2) governs the chemical sensitivity to interstitial flow. Moreover, in equation (1), D_b and f represent cells' diffusivity and growth/death rates, respectively. In equation (2), D_c governs the chemical signal's diffusivity, and g describes its production/degradation rates.

Recent studies have investigated how interstitial flow affects tumor cell dynamics. In [27], the authors use a multiphase cell migration model to study how ECM heterogeneities influence a tumor's metastatic propensity. In [22], the authors define a mechanobiological model to analyze the mechanical factors that drive cell migration, and in [16], the focus is on how a growing tumor responds to combination chemotherapy. In the experimental section of this article, we emphasize the interaction between ECM, interstitial flow, and chemical signal. We train a particular version of the model (1)-(5) to reproduce in vitro tumor cell migration results reported in [24].

We also focus on the convergence analysis of a fully discrete scheme for the Keller-Segel-Flow system (1)-(5). While previous studies (e.g., [17, 6, 8, 25, 28, 9, 10, 4, 3]) have explored the numerical discretization of Keller-Segel-Flow systems, many lack a theoretical numerical analysis. Exceptions include [25, 9, 10], [28], and [4], which provide error estimates for implicit-explicit (IMEX) time schemes combined with different spatial discretizations: finite element, discontinuous Galerkin, and a mixed finite volume-finite element approach. Here, the proposed fully discrete method for (1)-(5) combines finite difference in space with an IMEX scheme in time that handles the nonlinear and coupled terms. We add to the literature by establishing a sharp (with respect to solution regularity) second-order superconvergence estimate in space in a discrete H^1-norm. The proof is based on the Bramble-Hilbert lemma, avoiding the classical truncation error bound. Additionally, we provide an optimal first-order convergence estimate in

time in a discrete L^2-norm. This work builds on the analysis of elliptic equations presented in [13, 2] and followed, e.g., in [11, 12] for parabolic equations motivated by enhanced drug delivery.

We organize the paper as follows. In Section 2, we introduce the semidiscrete finite difference method (FDM) for (1)-(5) and establish its convergence and stability. Section 3 extends the analysis to the fully discrete scheme, combining FDM with implicit-explicit (IMEX) time integration. Section 4 focuses on numerical experiments. We present examples that confirm the theoretical error analysis and use system (1)-(5) to model in vitro tumor cell migration experiments. Section 5 concludes.

2 Semidiscrete FDM

Let Λ be a sequence of vectors $H = (h, k)$, $h = (h_1, h_2, \ldots, h_N), k = (k_1, k_2, \ldots, k_M)$, with $h_i > 0, i = 1, \ldots, N$, $k_j, j = 1, \ldots, M$, such that $\sum_{i=1}^{N} h_i = \sum_{j=1}^{M} k_j = 1$, and $H_{max} = \max\{h_{max}, k_{max}\} \to 0$, where $h_{max} = \max_{i=1,\ldots,N} h_i$, being k_{max} defined analogously.

We define the nonuniform finite difference grid

$$\overline{\Omega}_H = \{(x_i, y_j) : \underset{i=1,\ldots,N}{x_i} = x_{i-1} + h_i, \underset{j=1,\ldots,M}{y_j} = y_{j-1} + k_j\},$$

with $x_0 = y_0 = 0$, $x_N = y_M = 1$. We set $\Omega_H = \overline{\Omega}_H \cap \Omega$ and $\partial\Omega_H = \overline{\Omega}_H \cap \partial\Omega$. Let V_H be the set of grid functions defined in $\overline{\Omega}_H$ and let $V_{H,0}$ be the subset of grid functions in V_H that are null on $\partial\Omega_H$.

The proposed finite difference method (FDM) for system (1)-(5) is given by: find $c_{b,H}(t)$, $c_{c,H}(t) \in V_{H,0}$ and $p_H(t) \in V_H$, such that, for $t \in (0, T]$

$$\begin{cases} c'_{b,H}(t) + \nabla_{c,H} \cdot (\phi_H(t) c_{b,H}(t)) = \nabla^*_H \cdot (D_{b,H}(t) \nabla_H c_{b,H}(t)) + f_H(t), & (9) \\ c'_{c,H}(t) + \nabla_{c,H} \cdot (\psi_H(t) c_{c,H}(t)) = \nabla^*_H \cdot (D_{c,H}(t) \nabla_H c_{c,H}(t)) + g_H(t), & (10) \\ -\nabla^*_H \cdot (D_{p,H}(t) \nabla_H p_H(t)) = q_H(t), & (11) \end{cases}$$

with initial conditions (4) and boundary conditions (5).

Remark 1 *In (9)-(11), we consider the operators* $\nabla_H = (D_{-x}, D_{-y})$, $\nabla^*_H = (D^*_x, D^*_y)$, *and* $\nabla_{c,H} = (D_{c,x}, D_{c,y})$ *with*

$$D_{-x} u_H(x_i, y_j) = \frac{u_H(x_i, y_j) - u_H(x_{i-1}, y_j)}{h_i}, \qquad D_{c,x} u_H(x_i, y_j) = \frac{u_H(x_{i+1}, y_j) - u_H(x_{i-1}, y_j)}{h_i + h_{i+1}},$$

$$D^*_x u_H(x_i, y_j) = \frac{u_H(x_{i+1}, y_j) - u_H(x_i, y_j)}{h_{i+1/2}},$$

where $h_{i+1/2} = \frac{1}{2}(h_{i+1} + h_i)$ *and with the y-direction operators* D_{-y}, $D_{c,y}$, *and* D^*_y *analogously defined. We also define*

$$D_{b,H}(t) = \begin{bmatrix} D_{b,11}(M_h c_{b,H}(t), M_h c_{c,H}(t)) & 0 \\ 0 & D_{b,22}(M_k c_{b,H}(t), M_k c_{c,H}(t)) \end{bmatrix}, \qquad (12)$$

where

$$M_h u_H(x_i, y_j) = \frac{u_H(x_i, y_j) + u_H(x_{i-1}, y_j)}{2}, \tag{13}$$

and with the y-direction operator M_k analogously defined. The operators $D_{c,H}(t)$ and $D_{p,H}(t)$ are equivalently defined.

We also have

$$\phi_H(t) = \begin{bmatrix} \phi_1(D_h c_{c,H}(t), c_{c,H}(t), D_h p_H(t)) \\ \phi_2(D_k c_{c,H}(t), c_{c,H}(t), D_k p_H(t)) \end{bmatrix}^T, \qquad \psi_H(t) = \begin{bmatrix} \psi_1(D_h p_H(t)) \\ \psi_2(D_k p_H(t)) \end{bmatrix}^T. \tag{14}$$

where

$$D_h u_H(x_i, y_j) = \frac{h_i}{h_i + h_{i+1}} D_{-x} u_H(x_{i+1}, y_j) + \frac{h_{i+1}}{h_i + h_{i+1}} D_{-x} u_H(x_i, y_j),$$

and with the y-direction operator D_k analogously defined. Set also $f_H(t) = f(c_{b,H}(t), c_{c,H}(t))$, and analogously for $g_H(t)$ and $q_H(t)$.

2.1 Auxiliary results

Let us define the inner product

$$(u_H, w_H)_H = \sum_{(x_i, y_j) \in \Omega_H} h_{i+1/2} k_{j+1/2} u_H(x_i, y_j) w_H(x_i, y_j), \tag{15}$$

for $u_H, v_H \in V_{H,0}$, with $\|.\|_H$ the induced norm. Write

$$(u_H, w_H)_x = \sum_{i=1}^{N} \sum_{j=1}^{M-1} h_i k_{j+1/2} u_H(x_i, y_j) w_H(x_i, y_j),$$

and set $\|u_H\|_x^2 = (u_H, u_H)_x$. Analogously define $(u_H, w_H)_y$ and $\|u_H\|_y$, and consider

$$(u_H, w_H) = (u_{H,1}, w_{H,1})_x + (u_{H,2}, w_{H,2})_y, \tag{16}$$

and $\|u_H\|^2$, with obvious meaning. We have

$$\begin{aligned} \|\nabla_H u_H\|^2 &= \|D_{-x} u_H\|_x^2 + \|D_{-y} u_H\|_y^2 \\ &= (D_{-x} u_H, D_{-x} u_H)_x + (D_{-y} u_H, D_{-y} u_H)_y, \end{aligned}$$

and denote by $\|.\|_{1,H}$ the discrete $H^1(\Omega)$-norm

$$\|u_H\|_{1,H}^2 = \|u_H\|_H^2 + \|\nabla_H u_H\|^2, \quad u_H \in V_{H,0}. \tag{17}$$

Proposition 1 *(Discrete Poincaré inequality) It holds that*

$$\|u_H\|_H \leq \frac{1}{2} \|\nabla_H u_H\|, \quad \forall\, u_H \in V_{H,0}. \tag{18}$$

Proof: *Note that $u_H(x_i, y_j) = \sum_{m=1}^{i} h_m D_{-x} u_H(x_m, y_j)$.*

■

The next propositions follow by using summation by parts and some straightforward calculations.

Proposition 2 *For the diagonal matrix $D_{b,H}(t)$ in (9) (or $D_{c,H}(t)$ or $D_{p,H}(t)$), we have*

$$(\nabla_H^* \cdot (D_{b,H}(t)\nabla_H u_H), w_H)_H = -(D_{b,H}(t)\nabla_H u_H, \nabla_H w_H), \quad \forall\, w_H(t) \in V_{H,0}.$$

■

Proposition 3 *Consider $w_{H,1}, w_{H,2} \in V_{H,0}$, define $W_H = (w_{H,1}, w_{H,2})$, and recall the definition of $(\cdot,\cdot)$ (16). We set*

$$(M_H(W_H), W_H) = (M_h w_{H,1}, w_{H,1})_H + (M_k w_{H,2}, w_{H,2})_H,$$

with M_h, M_k as defined in (13). It holds

$$(\nabla_{c,H} \cdot W_H, w_H)_H = -(M_H(W_H), \nabla_H w_H), \quad \forall\, w_H \in V_{H,0}.$$

■

Using Propositions 2 and 3, we rewrite the FDM (9)-(11) in a form suitable for the upcoming convergence analysis. It reads: find $c_{b,H}(t)$, $c_{c,H}(t) \in V_{H,0}$ and $p_H(t) \in V_H$, such that, for $t \in (0,T]$

$$\begin{cases} (c'_{b,H}(t), w_{b,H})_H - (M_H(\phi_H(t)c_{b,H}(t)), \nabla_H w_{b,H}) = \\ \qquad\qquad - (D_{b,H}(t)\nabla_H c_{b,H}(t), \nabla_H w_{b,H}) + (f_H(t), w_{b,H})_H, & (19) \\ (c'_{c,H}(t), w_{c,H})_H - (M_H(\psi_H(t)c_{c,H}(t)), \nabla_H w_{c,H}) = \\ \qquad\qquad - (D_{c,H}(t)\nabla_H c_{c,H}(t), \nabla_H w_{c,H}) + (g_H(t), w_{c,H})_H, & (20) \\ (D_{p,H}(t)\nabla_H p_H(t), \nabla_H w_{p,H}) = (q_H(t), w_{p,H})_H, & (21) \end{cases}$$

for $w_{b,H}, w_{c,H}, w_{p,H} \in V_{H,0}$.

In the next section, we present our main result (Theorem 1), which states the second-order superconvergence of the FDM (9)-(11) in the discrete H^1-norm (17).

2.2 Convergence analysis

Let (c_b, c_c, p) be a solution of the Keller-Segel-Flow system (1)-(5) and $(c_{b,H}, c_{c,H}, p_H)$ an approximation obtained by the FDM (9)-(11). We consider the numerical error

$$E_{b,H}(t) = c_b(t) - c_{b,H}(t), t \in [0,T],$$

with analogous meaning for $E_{c,H}(t)$ and $E_{p,H}(t)$.

Remark 2 ***(Regularity assumptions)*** *We make the following assumptions on the nonuniform finite difference grid $\overline{\Omega}_H$ and the coefficient functions of the Keller-Segel-Flow system (1)-(5).*

(I) Let H be the family of finite difference grids, $H = (h, k) \in \Lambda$, with $H_{max} = max\{h_{max}, k_{max}\}$ and $H_{min} = min\{h_{min}, k_{min}\}$ with $h_{min} = \min_{i=1,\dots,N} h_i$ being k_{min} defined analogously. There exists C_g such that

$$\frac{H_{max}}{H_{min}} \leq C_g;$$

(II) The functions $\{D_{b,ii}\}_{i=1,2}$ (6) are Lipschitz with constant L_{D_b}, there exists $D_{b,0}$ such that $D_{b,ii} \geq D_{b,0} > 0$, and $D_{b,ii} \in W^{2,\infty}(\Omega)$ (analogously for D_c and D_p);

(III) The functions $\{\phi_i\}_{i=1,2}$ (7) are Lipschitz with constant L_ϕ, there exists C_ϕ such that $|\phi_i| \leq C_\phi$, and $(\phi_1(t)c_b(t), \phi_2(t)c_b(t)) \in [H^2(\Omega)]^2$ (analogously for ψ (8));

(IV) The function f is Lipschitz with constant L_f and $f(t) = f(c_b(t), c_c(t)) \in H^2(\Omega)$ (analogously for g and q).

Similar assumptions regarding the mesh (quasi-uniformity) and the coefficient functions are common in the literature, particularly in the analysis of coupled nonlinear systems (see, e.g., [10, 4, 25, 3]). Here and hereafter, C and L, with or without subscripts, denote positive constants independent of mesh parameters. Without loss of generality, the value of the constants may differ at different occurrences.

If $c : \overline{\Omega} \times [0, T] \to \mathbb{R}$, then, for $t \in [0, T]$, we use the notation $c(t) : \overline{\Omega} \to \mathbb{R}$, with $c(t)(x, y) = c(x, y, t)$. Analogously, for $t \in [0, T]$, $c^{(j)}(t) : \overline{\Omega} \to \mathbb{R}$, is given by $c^{(j)}(t)(x, y) = \dfrac{\partial^j c}{\partial t^j}(x, y, t)$, $j \in \mathbb{N}$.

Proposition 4 *(**Estimate for $E_{b,H}(t)$**) Assume that the assumptions of Remark 2 hold. If $c_b(t), c_c(t), p(t) \in H^3(\Omega)$ and $c_b'(t) \in H^2(\Omega)$, then*

$$\begin{aligned}
\frac{d}{dt}\|E_{b,H}(t)\|_H^2 &+ (D_{b,0} - \epsilon_b^2)\|\nabla_H E_{b,H}(t)\|^2 \\
&\leq \frac{1}{\epsilon_b^2} C_g L_\phi \|c_b(t)\|^2_{C^0(\overline{\Omega})}(\|E_{c,H}(t)\|^2_{1,H} + \|\nabla_H E_{p,H}(t)\|^2) \\
&\quad + \frac{1}{\epsilon_b^2}(C_\phi \|E_{b,H}(t)\|_H^2 + L_{D_b}\|c_b(t)\|^2_{C^1(\overline{\Omega})}(\|E_{b,H}(t)\|_H^2 + \|E_{c,H}(t)\|_H^2)) \\
&\quad + L_f(\|E_{b,H}(t)\|_H + \|E_{c,H}(t)\|_H)\|E_{b,H}(t)\|_H + T_{b,H}(t), \qquad (22)
\end{aligned}$$

with $\epsilon_b \neq 0$, and

$$\begin{aligned}
T_{b,H}(t) = CH^4_{max}(&\|f(t)\|^2_{H^2(\Omega)} + \|c_b'(t)\|^2_{H^2(\Omega)} + \|c_b(t)\|^2_{H^3(\Omega)} + \|c_c(t)\|^2_{H^3(\Omega)} + \|p(t)\|^2_{H^3(\Omega)} \\
&+ \|\phi(t)c_b(t)\|^2_{[H^2(\Omega)]^2} + \|c_c(t)c_b(t)\|^2_{H^3(\Omega)} + \|p(t)c_b(t)\|^2_{H^2(\Omega)}). \qquad (23)
\end{aligned}$$

Proof: We split the proof into three steps. Step 1 involves the definition of a suitable equation for $E_{b,H}(t)$ using the FDM with formulation (19)-(21) and the Keller-Segel-Flow system (1)-(5). In Steps 2 and 3, we bound the equation obtained in Step 1 using the regularity assumptions on Remark 2 and Bramble-Hilbert lemma.

Step 1. Taking in (19) $w_{b,H} = E_{b,H}(t)$, we get

$$(c'_{b,H}(t), E_{b,H}(t))_H - (M_H(\phi_H(t)c_{b,H}(t)), \nabla_H E_{b,H}(t)) = \\ - (D_{b,H}(t)\nabla_H c_{b,H}(t), \nabla_H E_{b,H}(t)) + (f_H(t), E_{b,H}(t))_H. \tag{24}$$

On the other hand, from the Keller-Segel-Flow equation (1), we get

$$((c'_b(t))_H, E_{b,H}(t))_H + ((\nabla \cdot (\phi(t)c_b(t)))_H, E_{b,H}(t))_H = \\ ((\nabla \cdot (D_b(t)\nabla c_b(t)))_H, E_{b,H}(t))_H + ((f(t))_H, E_{b,H}(t))_H, \tag{25}$$

where, e.g.,

$$(c'_b(t))_H = \frac{1}{h_{i+1/2}k_{j+1/2}} \int_{x_{i-1/2}}^{x_{i+1/2}} \int_{y_{j-1/2}}^{y_{j+1/2}} c'_b(x,y,t)\, dxdy,$$

Let us define $\widetilde{D}_{b,H}(t)$ and $\widetilde{\phi}_H(t)$ like in (12) and (14), but replacing the numerical approximations $c_{b,H}(t)$, $c_{c,H}(t)$, $p_H(t)$ by $c_b(t)$, $c_c(t)$, $p(t)$. Next, by adding and subtracting

$$(c'_b(t), E_{b,H}(t))_H, \qquad (M_H(\widetilde{\phi}_H(t)c_b(t)), \nabla_H E_{b,H}(t)),$$

$$(\widetilde{D}_{b,H}(t)\nabla_H c_b(t), \nabla_H E_{b,H}(t)), \qquad (f(t), E_{b,H}(t))_H,$$

to (25), one gets

$$(c'_b(t), E_{b,H}(t))_H - (M_H(\widetilde{\phi}_H(t)c_b(t)), \nabla_H E_{b,H}(t)) = \\ - (\widetilde{D}_{b,H}(t)\nabla_H c_b(t), \nabla_H E_{b,H}(t)) + (f(t), E_{b,H}(t))_H + \sum_{\ell=1}^{4} T_{b,H}^{(\ell)}(t), \tag{26}$$

where

$$T_{b,H}^{(1)}(t) = -((\nabla \cdot (\phi(t)c_b(t)))_H, E_{b,H}(t))_H - (M_H(\widetilde{\phi}_H(t)c_b(t)), \nabla_H E_{b,H}(t)),$$
$$T_{b,H}^{(2)}(t) = ((\nabla \cdot (D_b(t)\nabla c_b(t)))_H, E_{b,H}(t))_H + (\widetilde{D}_{b,H}(t)\nabla_H c_b(t), \nabla_H E_{b,H}(t)),$$
$$T_{b,H}^{(3)}(t) = ((f(t))_H - f(t), E_{b,H}(t))_H,$$
$$T_{b,H}^{(4)}(t) = (c'_b(t) - (c'_b(t))_H, E_{b,H}(t))_H.$$

Equations (24) and (26), yield

$$\frac{1}{2}\frac{d}{dt}\|E_{b,H}(t)\|_H^2 + (D_{b,H}(t)\nabla_H E_{b,H}(t), \nabla_H E_{b,H}(t)) = (M_H(\phi_H(t)E_{b,H}(t)), \nabla_H E_{b,H}(t)) \\ - (M_H((\phi_H(t) - \widetilde{\phi}_H(t))c_b(t)), \nabla_H E_{b,H}(t)) \\ - ((D_{b,H}(t) - \widetilde{D}_{b,H}(t))\nabla_H c_b(t), \nabla_H E_{b,H}(t)) \\ + (f_H(t) - f(t), E_{b,H}(t))_H - \sum_{\ell=1}^{4} T_{b,H}^{(\ell)}(t). \tag{27}$$

■

Step 2. Here, we bound some terms in (27). From assumption Remark 2(II), we obtain

$$(D_{b,H}(t)\nabla_H E_{b,H}(t), \nabla_H E_{b,H}(t)) \geq D_{b,0}\|\nabla_H E_{b,H}(t)\|^2, \tag{28}$$

and

$$\begin{aligned} -((D_{b,H}(t) - \widetilde{D}_{b,H}(t))\nabla_H c_b(t), \nabla_H E_{b,H}(t)) \\ \leq L_{D_b}\|c_b(t)\|_{C^1(\overline{\Omega})}\sqrt{2}(\|E_{b,H}(t)\|_H + \|E_{c,H}(t)\|_H)\|\nabla_H E_{b,H}(t)\|. \end{aligned} \tag{29}$$

Assumptions Remark 2(I) and Remark 2(III), give

$$(M_H(\phi_H(t)E_{b,H}(t)), \nabla_H E_{b,H}(t)) \leq \sqrt{2}C_\phi\|E_{b,H}(t)\|_H\|\nabla_H E_{b,H}(t)\|, \tag{30}$$

and

$$\begin{aligned} &- (M_H((\phi_H(t) - \widetilde{\phi}_H(t))c_b(t)), \nabla_H E_{b,H}(t)) \\ &\leq L_\phi\|c_b(t)\|_{C^0(\overline{\Omega})}(2C_g + 1)(\|\nabla_H E_{c,H}(t)\| + \|E_{c,H}(t)\|_H + \|\nabla_H E_{p,H}(t)\|)\|\nabla_H E_{b,H}(t)\|. \end{aligned} \tag{31}$$

Assumption Remark 2(IV), yields

$$(f_H(t) - f(t), E_{b,H}(t))_H \leq L_f(\|E_{b,H}(t)\|_H + \|E_{c,H}(t)\|_H)\|E_{b,H}(t)\|_H. \tag{32}$$

■

Step 3. Here, we estimate the terms $T_{b,H}^{(\ell)}(t)$, $\ell = 1, \ldots, 4$, in (27).

• For $T_{b,H}^{(3)}(t)$ and $T_{b,H}^{(4)}(t)$, lemma 5.7 in [13], gives

$$|T_{b,H}^{(3)}(t)| \leq CH_{max}^2\|f(t)\|_{H^2(\Omega)}\|\nabla_H E_{b,H}(t)\|, \tag{33}$$

and

$$|T_{b,H}^{(4)}(t)| \leq CH_{max}^2\|c_b'(t)\|_{H^2(\Omega)}\|\nabla_H E_{b,H}(t)\|. \tag{34}$$

■

• For $T_{b,H}^{(1)}(t)$, we have

$$\begin{aligned} T_{b,H}^{(1)}(t) &= -((\nabla \cdot (\phi(t)c_b(t)))_H, E_{b,H}(t))_H - (M_H(\phi(t)c_b(t)), \nabla_H E_{b,H}(t)) \\ &\qquad + (M_H(\phi(t)c_b(t)) - M_H(\widetilde{\phi}_H(t)c_b(t)), \nabla_H E_{b,H}(t)) \\ &:= T_{b,1}^{(1)}(t) + T_{b,2}^{(1)}(t), \end{aligned}$$

and lemma 5.5 in [13], gives

$$|T_{b,1}^{(1)}(t)| \leq CH_{max}^2\|\phi(t)c_b(t)\|_{[H^2(\Omega)]^2}\|\nabla_H E_{b,H}(t)\|. \tag{35}$$

Using Proposition 3 and definition (16) to expand $T_{b,2}^{(1)}(t)$, and applying afterward the Lipschitz assumption (Remark 2(III)) to $\phi(t)$, we find that estimating $T_{b,2}^{(1)}(t)$ is equivalent to estimate

$$\sum_{(x_i,y_j)\in\Omega_H} h_i k_{j+1/2}\left(\frac{\partial c_c}{\partial x}(x_i, y_j, t) - D_h c_c(x_i, y_j, t)\right)c_b(x_i, y_j, t)D_{-x}E_{b,H}(x_i, y_j, t), \tag{36}$$

$$\sum_{(x_i,y_j)\in\Omega_H} h_i k_{j+1/2}(\frac{\partial p}{\partial x}(x_i,y_j,t) - D_h p(x_i,y_j,t))c_b(x_i,y_j,t)D_{-x}E_{b,H}(x_i,y_j,t),$$

and two analogous expressions in the y-direction. Because all these terms can be estimated identically, we focus only on (36). However, we make use of this similarity in obvious steps. Setting

$$\theta(x_i,y_j,t) := (\frac{\partial c_c}{\partial x}(x_i,y_j,t) - D_h c_c(x_i,y_j,t))c_b(x_i,y_j,t),$$

one gets

$$\begin{aligned}\sum_{(x_i,y_j)\in\Omega_H} & h_i k_{j+1/2}|\theta(x_i,y_j,t)||D_{-x}E_{b,H}(x_i,y_j,t)| \\ &\leq \sum_{(x_i,y_j)\in\Omega_H} h_i|k_{j+1/2}\theta(x_i,y_j,t) - \int_{y_{j-1/2}}^{y_{j+1/2}}\theta(x_i,y,t)\,dy||D_{-x}E_{b,H}(x_i,y_j,t)| \\ &\qquad + \sum_{(x_i,y_j)\in\Omega_H} h_i\int_{y_{j-1/2}}^{y_{j+1/2}}|\theta(x_i,y,t)|\,dy|D_{-x}E_{b,H}(x_i,y_j,t)|. \quad (37)\end{aligned}$$

Following the proof of lemma 5.1 in [13], yields

$$\begin{aligned}\sum_{(x_i,y_j)\in\Omega_H} & h_i|k_{j+1/2}\theta(x_i,y_j,t) - \int_{y_{j-1/2}}^{y_{j+1/2}}\theta(x_i,y,t)\,dy||D_{-x}E_{b,H}(x_i,y_j,t)| \\ &\leq CH_{max}^2\|c_c(t)c_b(t)\|_{H^3(\Omega)}\|\nabla_H E_{b,H}(t)\|. \quad (38)\end{aligned}$$

On the other hand, for the second term on the right-hand side of (37), we have

$$\begin{aligned}\theta(x_i,y_j,t) &:= \frac{\partial c_c}{\partial x}(x_i,y_j,t) - D_h c_c(x_i,y_j,t))c_b(x_i,y_j,t) \\ &= (\frac{\partial c_c}{\partial x}(x_i,y_j,t) - \rho\int_{x_{i-1}}^{x_i}\frac{\partial c_c}{\partial x}(x,y_j,t)\,dx - (1-\rho)\int_{x_i}^{x_{i+1}}\frac{\partial c_c}{\partial x}(x,y_j,t)\,dx)c_b(x_i,y_j,t),\end{aligned}$$

with $\rho = h_{i+1}/(h_i+h_{i+1})$, which gives

$$\begin{aligned}\int_{y_{j-1/2}}^{y_{j+1/2}}|\theta(x_i,y,t)|\,dy &= \frac{1}{h_i+h_{i+1}}\int_{y_{j-1/2}}^{y_{j+1/2}}|\frac{\partial c_c}{\partial x}(x_i,y,t)(h_i+h_{i+1}) \\ &\quad - \hat{\rho}(c_c(x_i,y,t) - c_c(x_{i-1},y,t)) - \frac{1}{\hat{\rho}}(c_c(x_{i+1},y,t) - c_c(x_i,y,t))||c_b(x_i,y,t)|\,dy,\end{aligned}$$

with $\hat{\rho} = h_{i+1}/h_i$. By applying the Bramble-Hilbert lemma to the functional $\lambda : W^{3,1}(0,1) \to \mathbb{R}$ given by

$$\lambda(v) := v'(\frac{1}{1+\hat{\rho}}) - \hat{\rho}(v(\frac{1}{1+\hat{\rho}}) - v(0)) - \frac{1}{\hat{\rho}}(v(1) - v(\frac{1}{1+\hat{\rho}})),$$

with $v(\xi) = c_c(x_{i-1} + \xi(h_i+h_{i+1}), y, t)$, one gets

$$\begin{aligned}\sum_{(x_i,y_j)\in\Omega_H} & h_i\int_{y_{j-1/2}}^{y_{j+1/2}}|\theta(x_i,y,t)|\,dy|D_{-x}E_{b,H}(x_i,y_j,t)| \\ &\leq CH_{max}^2\|c_b(t)\|_{C^0(\overline{\Omega})}\|c_c(t)\|_{H^3(\Omega)}\|\nabla_H E_{b,H}(t)\|. \quad (39)\end{aligned}$$

Combining (38),(39) for $T_{b,2}^{(1)}(t)$ and (35) for $T_{b,1}^{(1)}(t)$, gives

$$|T_{b,H}^{(1)}(t)| \leq CH_{max}^2(\|\phi(t)c_b(t)\|_{[H^2(\Omega)]^2} + \|c_b(t)\|_{C^0(\overline{\Omega})}(\|c_c(t)\|_{H^3(\Omega)} + \|p(t)\|_{H^3(\Omega)}) + \|c_c(t)c_b(t)\|_{H^3(\Omega)} + \|p(t)c_b(t)\|_{H^3(\Omega)})\|\nabla_H E_{b,H}(t)\|. \quad (40)$$

■

• For $T_{b,H}^{(2)}(t)$, let $\widehat{D}_b$ be like in (6), but with

$$\widehat{D}_{b,11}(c_b(x_i, y_j, t), c_c(x_i, y_j, t)) = D_{b,11}(c_b(x_{i-1/2}, y_j, t), c_c(x_{i-1/2}, y_j, t)),$$

and analogously for $\widehat{D}_{b,22}$. Adding and subtracting

$$(\widehat{D}_b(t)\nabla_H c_b(t), \nabla_H E_{b,H}(t)),$$

to $T_{b,H}^{(2)}(t)$, yields

$$\begin{aligned} T_{b,H}^{(2)}(t) &= ((\nabla \cdot (D_b(t)\nabla c_b(t)))_H, E_{b,H}(t)) + (\widehat{D}_b(t)\nabla_H c_b(t), \nabla_H E_{b,H}(t)) \\ &\quad - ((\widehat{D}_b(t) - \widetilde{D}_{b,H}(t))\nabla_H c_b(t)), \nabla_H E_{b,H}(t)), \\ &:= T_{b,1}^{(2)}(t) + T_{b,2}^{(2)}(t). \end{aligned}$$

For $T_{b,1}^{(2)}(t)$, by lemma 5.1 in [13], we have

$$|T_{b,1}^{(2)}(t)| \leq CH_{max}^2\|c_b(t)\|_{H^3(\Omega)}\|\nabla_H E_{b,H}(t)\|. \quad (41)$$

Using Proposition 3 and definition (16) to expand $T_{b,2}^{(2)}(t)$, and applying afterward the Lipschitz assumption (Remark 2(II)) to $D_b(t)$, we find that estimating $T_{b,2}^{(2)}(t)$ is equivalent to estimate

$$\sum_{(x_i,y_j)\in\Omega_H} h_i k_{j+1/2}(c_b(x_{i-1/2}, y_j, t) - M_h c_b(x_i, y_j, t))D_{-x}c_b(x_i, y_j, t)D_{-x}E_{b,H}(x_i, y_j, t), \quad (42)$$

$$\sum_{(x_i,y_j)\in\Omega_H} h_i k_{j+1/2}(c_c(x_{i-1/2}, y_j, t) - M_h c_c(x_i, y_j, t))D_{-x}c_b(x_i, y_j, t)D_{-x}E_{b,H}(x_i, y_j, t),$$

and two analogous expressions in the y-direction. Because all these terms can be estimated identically, we focus only on (42). However, we make use of this similarity in obvious steps. Recalling, that $M_h c_b(x_i, y_j, t) = (c_b(x_{i-1}, y_j, t) + c_b(x_i, y_j, t))/2$, we bound

$$|c_b(x_{i-1/2}, y_j, t) - M_h c_b(x_i, y_j, t)|$$

by applying the Bramble-Hilbert lemma to the functional $\lambda : W^{2,1}((0,1)^2) \to \mathbb{R}$ defined by

$$\lambda(v) := v(\frac{1}{2}, 1) - \frac{1}{2}(v(0,1) + v(1,1)),$$

with $v(\xi,\gamma) = c_b(x_{i-1}+\xi h_i, y_{j-1}+\gamma k_j, t)$, yielding

$$|T^{(2)}_{b,2}(t)| \leq CH^2_{max}(\|c_b(t)\|_{H^2(\Omega)} + \|c_c(t)\|_{H^2(\Omega)})\|c_b(t)\|_{C^1(\overline{\Omega})}\|\nabla_H E_{b,H}(t)\|. \tag{43}$$

Combining (43) for $T^{(2)}_{b,2}(t)$ and (41) for $T^{(2)}_{b,1}(t)$, gives

$$\begin{aligned}|T^{(2)}_{b,H}(t)| \leq CH^2_{max}(&\|c_b(t)\|_{H^3(\Omega)} \\ &+ (\|c_b(t)\|_{H^2(\Omega)} + \|c_c(t)\|_{H^2(\Omega)})\|c_b(t)\|_{C^1(\overline{\Omega})}\|)\nabla_H E_{b,H}(t)\|.\end{aligned} \tag{44}$$

To finish the proof of Proposition 4, we collect estimates (33),(34),(40),(44) related with $T_{b,H}(t)$, use (28)-(32) to bound (27), and multiple applications of Young's inequality with ϵ lead to (23) and (22). It should be pointed out that taking into account the embedding of $H^3(\Omega)$ in $C^1(\overline{\Omega})$ then $c_b(t) \in C^1(\overline{\Omega})$.

■

By adapting the proof of Proposition 4, one can derive the following propositions for $E_{c,h}(t)$ and $E_{p,h}(t)$.

Proposition 5 *(**Estimate for $E_{c,H}(t)$**) Assume that the assumptions of Remark 2 hold. If $c_c(t), p(t) \in H^3(\Omega)$ and $c_b(t), c_c'F(t) \in H^2(\Omega)$, then*

$$\begin{aligned}&\frac{d}{dt}\|E_{c,H}(t)\|^2_H + (D_{c,0} - \epsilon_c^2)\|\nabla_H E_{c,H}(t)\|^2 \\ &\qquad\leq \frac{1}{\epsilon_c^2}C_g L_\psi \|c_c(t)\|^2_{C^0(\overline{\Omega})}\|\nabla_H E_{p,H}(t)\|^2 \\ &\qquad\quad + \frac{1}{\epsilon_c^2}(C_\psi\|E_{c,H}(t)\|^2_H + L_{D_c}\|c_c(t)\|^2_{C^1(\overline{\Omega})}(\|E_{b,H}(t)\|^2_H + \|E_{c,H}(t)\|^2_H)) \\ &\qquad\quad + L_g(\|E_{b,H}(t)\|_H + \|E_{c,H}(t)\|_H)\|E_{c,H}(t)\|_H + T_{c,H}(t),\end{aligned} \tag{45}$$

with $\epsilon_c \neq 0$, and

$$\begin{aligned}T_{c,H}(t) = CH^4_{max}(&\|g(t)\|^2_{H^2(\Omega)} + \|c_c'(t)\|^2_{H^2(\Omega)} + \|c_b(t)\|^2_{H^2(\Omega)} + \|c_c(t)\|^2_{H^3(\Omega)} + \|p(t)\|^2_{H^3(\Omega)} \\ &+ \|\psi(t)c_c(t)\|^2_{[H^2(\Omega)]^2} + \|p(t)c_c(t)\|^2_{H^3(\Omega)}).\end{aligned} \tag{46}$$

■

Proposition 6 *(**Estimate for $E_{p,H}(t)$**) Assume that the assumptions of Remark 2 hold. If $p(t) \in H^3(\Omega)$ and $c_b(t), c_c(t) \in H^2(\Omega)$, then*

$$\begin{aligned}&(D_{p,0} - L_q - \epsilon_p^2)\|\nabla_H E_{p,H}(t)\|^2 \\ &\qquad\leq \frac{1}{\epsilon_p^2}(L_{D_p}\|p(t)\|^2_{C^1(\overline{\Omega})} + L_q)(\|E_{b,H}(t)\|^2_H + \|E_{c,H}(t)\|^2_H) + T_{p,H}(t),\end{aligned} \tag{47}$$

with $\epsilon_p \neq 0$, and

$$T_{p,H}(t) = CH^4_{max}(\|q(t)\|^2_{H^2(\Omega)} + \|p(t)\|^2_{H^3(\Omega)} + \|c_b(t)\|^2_{H^2(\Omega)} + \|c_c(t)\|^2_{H^2(\Omega)}). \tag{48}$$

■

In Theorem 1, we establish our main result, the second-order convergence of the semi-discrete FDM (9)-(11). Since (9)-(11) has a truncation error of order one in the $\|.\|_\infty$-norm, this is a superconvergence result.

Theorem 1 *Assume that the assumptions of Remark 2 hold. If $c_b(t), c_c(t), p(t) \in H^3(\Omega)$ and $c_b'(t), c_c'(t) \in H^2(\Omega)$, then, for $t \in [0,T]$,*

$$\|E_{b,H}(t)\|_H^2 + \|E_{c,H}(t)\|_H^2 + \int_0^t \|\nabla_H E_{b,H}(s)\|^2 + \|\nabla_H E_{c,H}(s)\|^2 + \|\nabla_H E_{p,H}(s)\|^2 \, ds \leq C H_{max}^4 \int_0^t T_H(s)\, ds \tag{49}$$

with $\epsilon_b, \epsilon_c, \epsilon_p \neq 0$, such that

$$D_{b,0} - \epsilon_b^2 > 0, \tag{50}$$

$$D_{c,0} - \epsilon_c^2 - \frac{1}{\epsilon_b^2} C_g L_\phi \|c_b(t)\|_{C^0(\overline{\Omega})}^2 > 0, \tag{51}$$

$$D_{p,0} - \epsilon_p^2 - C_g\left(\frac{1}{\epsilon_b^2} L_\phi \|c_b(t)\|_{C^0(\overline{\Omega})}^2 + \frac{1}{\epsilon_c^2} L_\psi \|c_c(t)\|_{C^0(\overline{\Omega})}^2\right) - L_q > 0, \tag{52}$$

and where $T_H(s)$ is the sum of (23),(46),(48).

Proof: *The proof follows collecting the estimates in Propositions 4, 5 and 6, and applying Gronwall's inequality (Lemma 2.1 in [7]).*

■

Remark 3 *Conditions (50)-(52) impose some compatibility conditions between the data of the Keller-Segel-Flow system (1)-(5). For instance, fixing*

$$\epsilon_b^2 = \frac{1}{2} D_{b,0}$$

satisfying (50), we have from (51)

$$\epsilon_c^2 < D_{c,0} - \frac{2}{D_{b,0}} C_g L_\phi \|c_b(t)\|_{C^0(\overline{\Omega})}^2,$$

meaning that

$$\|c_b(t)\|_{C^0(\overline{\Omega})}^2 < \frac{D_{b,0} D_{c,0}}{2 C_g L_\phi}. \tag{53}$$

Type (53) restrictions, which establish compatibility conditions between coefficient functions, numerical grid, and the theoretical solution, appear even in the analysis of simpler Keller-Segel-Flow systems (see, e.g., Theorem 2.1 in [14]).

Remark 4 *Following the steps of Theorem 1, and as a direct consequence of the Bramble-Hilbert lemma, the FDM (9)-(11) has first-order convergence rate if $c_b(t), c_c(t), p(t) \in H^2(\Omega)$.*

Remark 5 *(**Stability analysis**) Let $c_{b,0}, c_{c,0}, p_0$ and $\widetilde{c}_{b,0}, \widetilde{c}_{c,0}, \widetilde{p}_0$ be two initial conditions of the FDM (9)-(11), denote by $c_{b,H}(t), c_{c,H}(t), p_H(t)$ and $\widetilde{c}_{b,H}(t), \widetilde{c}_{c,H}(t), \widetilde{p}_H(t)$ the corresponding numerical approximations, and define*

$$w_{c,H}(t) = c_{c,H}(t) - \widetilde{c}_{c,H}(t),$$

with analogous meaning for $w_{b,H}(t)$ and $w_{p,H}(t)$. Following the notion of mesh-dependent stability of López-Marcos and Sanz-Serna [18, 20], the FDM (9)-(11) is stable if, for all $\epsilon > 0$, there exists a mesh-dependent constant C_H such that if

$$\|\omega_{i,H}(0)\|_H \leq C_H \quad \textit{then} \quad \|\omega_{i,H}(t)\|_H \leq \epsilon, \quad i = c, b, p. \tag{54}$$

In other words, in the sense of (54), stability means that small perturbations in the initial conditions lead to small changes in the corresponding numerical solutions.

Note that under the assumptions of Theorem 1, it holds

$$\begin{aligned} \|c_{c,H}(t)\|_\infty^2 &\leq 2\|E_{c,H}(t)\|_\infty^2 + 2\|c_c(t)\|_\infty^2 \\ &\leq \frac{2}{H_{min}^2}\|E_{c,H}(t)\|_H^2 + 2\|c_c(t)\|_\infty^2 \\ &\leq CH_{max}^2 + 2\|c_c(t)\|_\infty^2 \qquad \textit{(Remark 2(I))} \\ &\leq C_H \end{aligned} \tag{55}$$

and

$$\int_0^t \|\nabla_H c_{c,H}(s)\|_\infty^2 \, ds \leq C_H, \tag{56}$$

with analogous estimates for $c_{b,H}(t)$ and $p_H(t)$. Then, following the steps of Theorem 1 (replacing $E_{i,H}(t)$ with $w_{i,H}(t)$, $i = c, b, p$), one can show that the FDM (9)-(11) is stable in the sense of (54).

3 Fully Discrete IMEX-FDM

This section presents an IMEX time integration for the FDM (9)-(11), thus yielding a fully discrete IMEX-FDM for system (1)-(5). In the time domain $[0, T]$, we define the uniform grid $t_n = t_{n-1} + \Delta t$, for $n = 1, \ldots, \mathcal{N}$, with $\Delta t > 0$ the time-step and $t_0 = 0$, $t_{\mathcal{N}} = T$. The proposed IMEX-FDM is given by: find $c_{b,H}^n$, $c_{c,H}^n \in V_{H,0}$ and $p_H^n \in V_H$, such that, for $n = 1, \ldots, \mathcal{N} - 1$,

$$\begin{cases} -\nabla_H^* \cdot (D_{p,H}^n \nabla_H p_H^{n+1}) = q_H^n, & (57) \\ D_{-t} c_{c,H}^{n+1} + \nabla_{c,H} \cdot (\psi_H^{n+1} c_{c,H}^{n+1}) = \nabla_H^* \cdot (D_{c,H}^n \nabla_H c_{c,H}^{n+1}) + g_H^n, & (58) \\ D_{-t} c_{b,H}^{n+1} + \nabla_{c,H} \cdot (\phi_H^{n+1} c_{b,H}^{n+1}) = \nabla_H^* \cdot (D_{b,H}^n \nabla_H c_{b,H}^{n+1}) + f_H^n, & (59) \end{cases}$$

with initial conditions (4) and boundary conditions (5).

Remark 6 *Most of the notation used in (57)-(59) is given in Remark 1 on page 3. Here, we introduce the operator $D_{-t} u_H^{n+1} = (u_H^{n+1} - u_H^n)/\Delta t$, and define $D_{p,H}^n$, $D_{c,H}^n$, and $D_{b,H}^n$ as in (12) but replacing $c_{b,H}(t)$ and $c_{c,H}(t)$ with $c_{b,H}^n$ and $c_{c,H}^n$, except for $D_{b,H}^n$ where we replace $c_{c,H}(t)$ with $c_{c,H}^{n+1}$. We also have ϕ_H^{n+1} and ψ_H^{n+1} as in (14) but replacing $p_H(t)$ and $c_{c,H}(t)$ with p_H^{n+1} and*

$c_{c,H}^{n+1}$. *We also set* $q_H^n = q(c_{b,H}^n, c_{c,H}^n, p_H^n)$, $g_H^n = g(c_{b,H}^n, c_{c,H}^n)$ *and* $f_H^n = f(c_{b,H}^n, c_{c,H}^{n+1})$. *This IMEX discretization, a combination of the explicit and implicit Euler scheme, avoids the solution of nonlinear systems.*

Theorem 2 establishes the first-order convergence rate of the IMEX-FDM (57)-(59).

Theorem 2 *Assume that the assumptions of Theorem 1 hold. If* $c_b, c_c, p \in C([0,T]; H^3(\Omega))$ *and* $c_b, c_c \in C^1([0,T]; H^2(\Omega)) \cap H^2(0,T; C(\overline{\Omega}))$, $f(c_b, c_c), g(c_b, c_c) \in H^1(0,T; C(\overline{\Omega}))$, *then, for* $n = 0, \ldots, \mathcal{N}-1$,

$$\|E_{b,H}^{n+1}\|_{1,H}^2 + \|E_{c,H}^{n+1}\|_{1,H}^2 + \|\nabla_H E_{p,H}^{n+1}\|^2 \leq C(H_{max}^4 + \Delta t^2) \tag{60}$$

with the mesh-independent time-step restriction $\Delta t < 1/C_{\Delta t}$, *where*

$$C_{\Delta t} = \frac{1}{\epsilon_p^2} L_{D_p} \|p\|_{C^{1,0}(\overline{\Omega}\times[0,T])}^2 + L_q + \frac{1}{\epsilon_c^2}\big(C_\psi + L_{D_c}\|c_c\|_{C^{1,0}(\overline{\Omega}\times[0,T])}^2 + L_g\big) + \frac{1}{\epsilon_b^2}\big(C_\phi + C_g L_\phi \|c_b\|_{C^0(\overline{\Omega}\times[0,T])}^2 + L_{D_b}\|c_b\|_{C^{1,0}(\overline{\Omega}\times[0,T])}^2 + L_f\big)$$

and $\epsilon_b, \epsilon_c, \epsilon_p \neq 0$ *are fixed by (50)-(52).*

Proof: *Let* $E_{b,H}^n = c_b(t_n) - c_{b,H}^n$, $n = 0, \ldots, \mathcal{N}$, *with analogous meaning for* $E_{c,H}^n$ *and* $E_{p,H}^n$. *The proof follows by establishing results equivalent to Propositions 4, 5, and 6 but now for the fully discrete IMEX-FDM (57)-(59). For example, analogously to Proposition 4,* $E_{b,H}^{n+1}$ *satisfies*

$$\begin{aligned}
&\|E_{b,H}^{n+1}\|_H^2 + \Delta t(D_{b,0} - \epsilon_b^2)\|\nabla_H E_{b,H}^{n+1}\|^2 \\
&\quad \leq \|E_{b,H}^n\|_H^2 + \Delta t \frac{1}{\epsilon_b^2} C_g L_\phi \|c_b(t_{n+1})\|_{C^0(\overline{\Omega})}^2 (\|E_{c,H}^{n+1}\|_{1,H}^2 + \|\nabla_H E_{p,H}^{n+1}\|^2) \\
&\quad\quad + \Delta t \frac{1}{\epsilon_b^2}(C_\phi \|E_{b,H}^{n+1}\|_H^2 + L_{D_b}\|c_b(t_{n+1})\|_{C^1(\overline{\Omega})}^2 (\|E_{b,H}^n\|_H^2 + \|E_{c,H}^{n+1}\|_H^2)) \\
&\quad\quad + \Delta t L_f (\|E_{b,H}^n\|_H + \|E_{c,H}^{n+1}\|_H)\|E_{b,H}^{n+1}\|_H + T_{b,\Delta t}^{n+1},
\end{aligned} \tag{61}$$

with $\epsilon_b \neq 0$, *and*

$$T_{b,\Delta t}^{n+1} = T_{b,H}(t_{n+1}) + C\Delta t^2 \int_{t_n}^{t_{n+1}} \|c_b(t_{n+1})\|_{C^1(\overline{\Omega})}^2 \big(\|c_b'(s)\|_H^2 + \|c_c'(s)\|_H^2\big) + \|c_b''(s)\|_H^2 + \|f'(s)\|_H^2 \, ds, \tag{62}$$

where $T_{b,H}(t_{n+1})$ *is the term of order* H_{max}^4 *defined by (23).*

To derive (61) we follow the steps of Proposition 4. We obtain

$$\begin{aligned}
(D_{-t}c_{b,H}^{n+1}, E_{b,H}^{n+1})_H - (M_H(\phi_H^{n+1} c_{b,H}^{n+1}), \nabla_H E_{b,H}^{n+1}) = \\
- (D_{b,H}^n \nabla_H c_{b,H}^{n+1}, \nabla_H E_{b,H}^{n+1}) + (f_H^n, E_{b,H}^{n+1})_H
\end{aligned} \tag{63}$$

and

$$\begin{aligned}
(D_{-t}c_b(t_{n+1}), E_{b,H}^{n+1})_H - (M_H(\widetilde{\phi}_H(t_{n+1}) c_b(t_{n+1})), \nabla_H E_{b,H}^{n+1}) = \\
- (\widetilde{D}_{b,H}(t_n) \nabla_H c_b(t_{n+1}), \nabla_H E_{b,H}^{n+1}) + (f(t_n), E_{b,H}^{n+1})_H + \sum_{\ell=1}^{4} T_{b,\Delta t}^{(\ell)},
\end{aligned} \tag{64}$$

where

$$T^{(1)}_{b,\Delta t} = -((\nabla\cdot(\phi(t_{n+1})c_b(t_{n+1})))_H, E^{n+1}_{b,H})_H - (M_H(\widetilde{\phi}_H(t_{n+1})c_b(t_{n+1})), \nabla_H E^{n+1}_{b,H}),$$
$$T^{(2)}_{b,\Delta t} = ((\nabla\cdot(D_b(t_{n+1})\nabla c_b(t_{n+1})))_H, E^{n+1}_{b,H})_H + (\widetilde{D}_{b,H}(t_n)\nabla_H c_b(t_{n+1}), \nabla_H E^{n+1}_{b,H}),$$
$$T^{(3)}_{b,\Delta t} = ((f(t_{n+1}))_H - f(t_n), E^{n+1}_{b,H})_H,$$
$$T^{(4)}_{b,\Delta t} = (D_{-t}c_b(t_{n+1}) - (c_b'(t_{n+1}))_H, E^{n+1}_{b,H})_H.$$

Equations (63) and (64), yield

$$\begin{aligned}(D_{-t}E^{n+1}_{b,H}, E^{n+1}_{b,H})_H + (D^n_{b,H}\nabla_H E^{n+1}_{b,H}, \nabla_H E^{n+1}_{b,H}) &= (M_H(\phi^{n+1}_H E^{n+1}_{b,H}), \nabla_H E^{n+1}_{b,H})\\ &- (M_H((\phi^{n+1}_H - \widetilde{\phi}_H(t_{n+1}))c_b(t_{n+1})), \nabla_H E^{n+1}_{b,H})\\ &- ((D^n_{b,H} - \widetilde{D}_{b,H}(t_n))\nabla_H c_b(t_{n+1}), \nabla_H E^{n+1}_{b,H})\\ &+ (f^n_H - f(t_n), E^{n+1}_{b,H})_H - \sum_{\ell=1}^{4} T^{(\ell)}_{b,\Delta t}. \end{aligned} \tag{65}$$

It can be shown that

$$|T^{(1)}_{b,\Delta t}| \le |T^{(1)}_{b,H}(t_{n+1})|, \tag{66}$$
$$|T^{(2)}_{b,\Delta t}| \le |T^{(2)}_{b,H}(t_{n+1})| + C\Delta t^2 \int_{t_n}^{t_{n+1}} \|c_b(t_{n+1})\|^2_{C^1(\overline{\Omega})}\left(\|c_b'(s)\|^2_H + \|c_c'(s)\|^2_H\right) ds, \tag{67}$$
$$|T^{(3)}_{b,\Delta t}| \le |T^{(3)}_{b,H}(t_{n+1})| + C\Delta t^2 \int_{t_n}^{t_{n+1}} \|f'(s)\|^2_H \, ds, \tag{68}$$
$$|T^{(4)}_{b,\Delta t}| \le |T^{(4)}_{b,H}(t_{n+1})| + C\Delta t^2 \int_{t_n}^{t_{n+1}} \|c_b''(s)\|^2_H \, ds, \tag{69}$$

where $|T^{(\ell)}_{b,H}(t_{n+1})|$, $\ell = 1,\ldots,4$, are bounded by terms of order H^4_{max} defined by (40), (44), (33), and (34). Collecting estimates (66)-(69), using inequalities analogous to (28)-(32) to bound (65), and resorting to Young's inequality with ϵ leads to (61) and (62).

Proceeding similarly, one can derive estimates analogous to (61) and (62) for $E^{n+1}_{c,h}$ and $E^{n+1}_{p,h}$. Collecting all the estimates, summing over n, and applying a discrete Gronwall's inequality (Lemma 4.3 in [7]), one can get (60).

■

Remark 7 ***(Stability analysis)*** *Assuming the restrictions $\Delta t/H^2_{max} \le C$ and $H^2_{max}/\Delta t \le C$, we can get estimates like (55),(56) for $c^n_{c,H}$, and one can show that the IMEX-FDM (57)-(59) is stable in a sense analogous to (54), i.e., with $w^n_{c,H} = c^n_{c,H} - \widetilde{c}^n_{c,H}$.*

4 Numerical Simulation

This section numerically illustrates the convergence results for the FDM in Theorem 1 and Remark 4, and for the IMEX-FDM in Theorem 2. We also model and simulate tumor cell migration using a system of PDEs of the form (1)-(5).

4.1 Accuracy of numerical solution

Example 1 *Let us consider system (1)-(5), for $t \in [0,1]$, with coefficients functions*

$$D_b = \begin{bmatrix} 1+c_c c_b & 0 \\ 0 & 2+c_b^2 \end{bmatrix}, \quad D_c = \begin{bmatrix} 1+c_c+c_b & 0 \\ 0 & 2+c_c^2 \end{bmatrix}, \quad D_p = \begin{bmatrix} 1+c_c+c_b & 0 \\ 0 & 1+c_b c_c \end{bmatrix},$$

$$\phi = \begin{bmatrix} \dfrac{\partial p}{\partial x} + \dfrac{\partial c_c}{\partial x} + c_c \\ \dfrac{\partial p}{\partial y} + \dfrac{\partial c_c}{\partial y} + c_c \end{bmatrix}, \quad \psi = \begin{bmatrix} \dfrac{\partial p}{\partial x} \\ \dfrac{\partial p}{\partial y} \end{bmatrix},$$

and $f(c_b, c_c) = c_b c_c^2$, $g(c_b, c_c) = c_b c_c$, and $q(c_b, c_c) = c_b + c_c$. We add suitable source functions to the system (1)-(5) such that, for $\alpha \in \mathbb{R}$, the exact solution of the problem is

$$\begin{aligned} c_b(x,y,t) &= e^{5t} xy(x-1)(y-1)|y-0.5|^\alpha, \\ c_c(x,y,t) &= e^{5t} xy(x-1)(y-1)|y-0.3|^\alpha, \\ p(x,y,t) &= 50xy(x-1)(y-1)|y-0.7|^\alpha. \end{aligned}$$

The solution (c_b, c_c, p) satisfies the regularity assumptions of Theorems 1 and 2 with $\alpha = 3.1$ and those of Remark 4 with $\alpha = 2.1$.

First, we analyze the rate of convergence in space. Starting with a random non-uniform spatial mesh, H_1, we successively solve Example 1 using in the iteration $k+1$ the mesh obtained by halving the previous mesh H_k, i.e., $H_{k+1} = H_k/2$. To ensure that the time error is negligible, we fix the time step of the order of H_{max}^2. Following the estimates in Theorem 1, we measure the numerical error by

$$Error_H^2 = \max_{n=0,\dots,\mathcal{N}-1} \|E_{b,H}^{n+1}\|_{1,H}^2 + \|E_{c,H}^{n+1}\|_{1,H}^2 + \|\nabla_H E_{p,H}^{n+1}\|^2,$$

and estimate the rate of convergence by

$$Rate = \log_2\left(\frac{Error_{H_k}}{Error_{H_{k+1}}}\right).$$

The numerical convergence rates in Table 1 agree with the theoretical convergence rates obtained in Theorem 1 and Remark 4.

Next, we analyze the rate of convergence in time. The procedure is similar, but here we fix a random space mesh with a small enough H_{max}, namely, $H_{max} = 3.1914\text{e-}03$, and we successively solve Example 1 (with $\alpha = 3.1$) using in the iteration $k+1$ the time step size $\Delta t_{k+1} = \Delta t_k/2$. The numerical convergence rate in Table 2 agrees with the theoretical first-order convergence rate obtained in Theorem 2.

4.2 Tumor cell migration: modeling and simulation

Understanding how tumor cells metastasize is crucial for developing effective cancer therapies. The lymphatic system's role as the primary vector for cancer metastasis is known; however, the phenomena underlying tumor cell migration toward the lymphatic capillaries remain unclear.

$\alpha = 3.1$			$\alpha = 2.1$		
H_{max}	$Error_H$	$Rate$	H_{max}	$Error_H$	$Rate$
2.0388e-01	6.2677e-01	-	1.8880e-01	9.5757e-01	-
1.0194e-01	1.5296e-01	2.0348	9.4399e-02	4.5462e-01	1.0747
5.0970e-02	4.0053e-02	1.9331	4.7199e-02	2.1322e-01	1.0923
2.5485e-02	9.8902e-03	2.0178	2.3600e-02	9.9101e-02	1.1054
1.2742e-02	2.4649e-03	2.0045	1.1800e-02	4.7725e-02	1.0542
6.3712e-03	6.1643e-04	1.9995	5.8999e-03	2.1776e-02	1.1320

Table 1: Rates of convergence in space for Example 1.

Δt	$Error_H$	$Rate$
2.0000e-01	1.5444e-01	0
1.0000e-01	9.0670e-02	7.6832e-01
5.0000e-02	4.9121e-02	8.8428e-01
2.5000e-02	2.5517e-02	9.4486e-01
1.2500e-02	1.2972e-02	9.7605e-01
6.2500e-03	6.5278e-03	9.9077e-01

Table 2: Rate of convergence in time for Example 1.

It's believed that this migration involves a complex interaction between tumor cells, chemokines, extracellular matrix (ECM), lymphatic endothelial cells (LECs), and interstitial flow (IF).

CCL21, a chemokine predominantly secreted by LECs and, to a lesser extent, by cancer cells, is emerging as a vital player in this dynamic. CCL21, essential for regulating immune responses, strongly binds to the sulfated proteoglycans in the ECM. Laboratory experiments suggest that tumor cells exploit the ECM-bound CCL21 to migrate. The reasoning is that tumor cell-secreted proteases interact with the ECM, releasing CCL21 and creating an extracellular chemokine gradient. Through the expression of the CCL21 receptor CCR7, tumor cells exploit this chemokine gradient to migrate toward the lymphatic capillaries. This movement of cells, known as autologous chemotaxis, is believed to be a dominant force behind tumor cell migration. Interstitial fluid (IF) flow from blood to lymphatic capillaries is another potentially relevant mechanism behind autologous chemotaxis. This flow, important for nutrient delivery and waste removal, can carry released CCL21, enhancing its gradient towards the lymphatics. The tumor's extra stress on the surrounding ECM may increase the IF, enhancing its impact [23, 19, 27, 26, 21, 24, 29, 15].

The laboratory work [23] investigates tumor cell migration under three scenarios: chemotaxis alone, chemotaxis with physiological flow, and static (without flow or chemokines). The study utilized a modified Boyden chamber assay:

- Top chamber: basal medium;
- Middle chamber: MDA-MB-435S tumor cells seeded in Matrigel;
- Bottom chamber: basal medium alone (static conditions) or with CCL21 (chemotaxis conditions).

The authors added CCL21 to the bottom chamber by culturing CCL21-secreting LECs to confluence for three days. To replicate the effect of interstitial flow, they established a water flow from the top to the bottom chamber. All experiments lasted 15 hours in a 37°C/5% CO_2 incubator. After this period, Matrigel was removed and the percentage of migrated cells was quantified.

Next, we present numerical simulations of tumor cell migration using a Keller-Segel-Flow model of type (1)-(5). We base our simulation setup on the laboratory experiment described in [23] and train our model using the reported experimental data. The model is given by

$$\begin{cases} \dfrac{\partial c_b}{\partial t} + \nabla \cdot (\chi c_b \nabla c_c) = D_b \Delta c_b & (70) \\ \dfrac{\partial c_c}{\partial t} + \nabla \cdot (v c_c) = D_c \Delta c_c + \alpha c_b c_{c,B} & (71) \\ -\nabla \cdot (K \nabla p) = q & (72) \end{cases}$$

where c_b denotes cell density, c_c free CCL21 concentration, and p pressure. In (72), q denotes a source term and K is the hydraulic conductivity. In (70), D_b denotes the cells' diffusion coefficient and χc_b represents the sensitivity to the gradient of the chemoattractant CCL21. To govern the evolution of the bound CCL21 ($c_{c,B}$), we define the ode $c'_{c,B}(t) = -\alpha c_b c_{c,B}$ with α the rate of bound-to-free CCL21 conversion. Note that a symmetric source term $\alpha c_b c_{c,B}$ appears in the free CCL21 equation (71). Given the relatively short duration of the experiments (15 h), we ignore the degradation/consumption of free CCL21. Still in (71), D_c represents the CCL21 diffusion coefficient, while the convection term $\nabla \cdot (v c_c)$ governs CCL21 transport under flow conditions, where $v = -K \nabla p$ denotes Darcy's velocity.

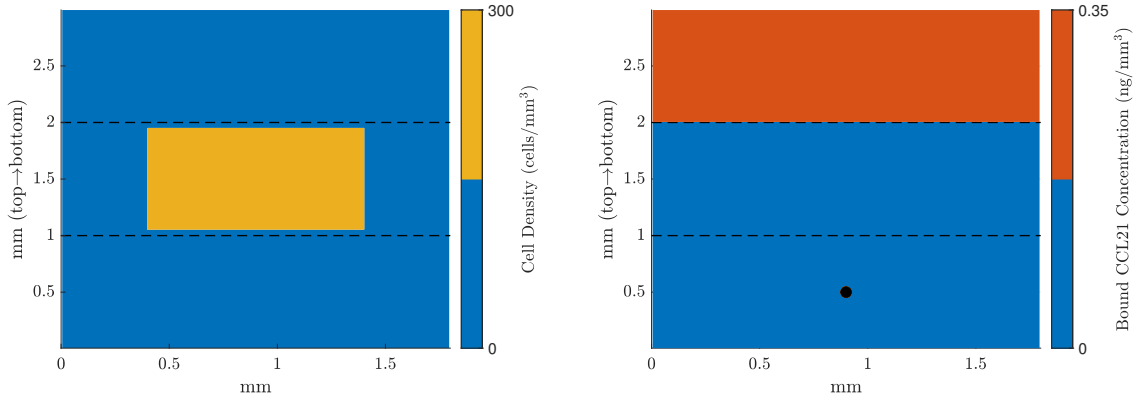

Figure 1: Schematic representation of the three-chambers computational domain and initial conditions. On the left: initial cell density in the middle chamber (delimited by the two horizontal dashed lines). On the right: initial bound CCL21 concentration on the bottom chamber. The dot indicates the location of the flow source in the top chamber. This setup replicates tumor cell migration toward LECs, i.e., from the top to the bottom chamber.

Figure 1 shows the computational domain and the initial conditions. We consider a three-chambers domain with tumor cells in the middle chamber and bound CCL21 in the bottom chamber. We assume an initial cell density of 300 cells/mm^3 and a bound CCL21 concentration of 0.35 ng/mm^3. Initially, all CCL21 is in the bound state. Since we are interested in measuring the percentage of cells migrated, the exact initial conditions, which are unknown, are less relevant. We assume homogeneous Dirichlet boundary conditions for Darcy's equation and simulate

flow conditions by a source term localized in the top chamber

$$q = \begin{cases} q_0 & \text{if } (x-0.9)^2 + (y-0.5)^2) < r^2 \quad (r = 0.3\,mm) \\ 0 & \text{otherwise} \end{cases} \tag{73}$$

with q_0 a source parameter and r the source radius fixed at 0.3 mm. We set homogeneous Dirichlet boundary conditions for CCL21 at the bottom boundary, simulating CCL21 washout. Due to the short experiment duration (15 h), we also set homogeneous Dirichlet boundary conditions for cell density and CCL21 at other boundaries, as they don't significantly affect the simulations. The model (70)-(73) parameter values are given in Table 3.

Par.	Unit	Value	Description	Typical Range
D_b	mm^2/h	5.3e-5	Cell diffusion coefficient	3.6e-6 mm^2/h - 3.6e-4 mm^2/h [5]
D_c	mm^2/h	4.2e-2	CCL21 diffusion coefficient	3.6e-1 mm^2/h - 3.6e-4 mm^2/h [5]
χ	mm^2/h	0.15	Chemotaxis coefficient	0.001-1 [5]
α	mm^5/ng-h	0.1	Rate of CCL21 conversion	-
K	mm^2/Pa-h	1	Hydraulic conductivity	Fixed
q_0	1/h	22	Flow source parameter	-

Table 3: Parameters used in the Keller-Segel-Flow system (70)-(73). Without loss of generality due to the linearity of equation (72), we fixed the medium hydraulic conductivity at $K = 1$. We optimized the remaining parameters to fit the experimental data in [23]. When available, we take typical values as a reference for the optimization. Using $q_0 = 22$ 1/h in Darcy's equation (72),(73), the mean absolute velocity $|v|$ in the tumor cell chamber is 0.74 mm/h, within the typical range of values for interstitial velocity, 0.36 mm/h - 7.2 mm/h [26].

Following the experimental setup in [23], we performed cell migration simulations under three conditions:

- Static: without chemokine CCL21 or flow, i.e., $c_{c,B}(0) = 0$ ng/mm^3 and $v = 0$ m/h;
- Chemotaxis: with chemokine CCL21, i.e., $c_{c,B}(0) = 0.35$ ng/mm^3 and $v = 0$ m/h;
- Chemotaxis and flow: with chemokine CCL21 and flow, i.e., $c_{c,B}(0) = 0.35$ ng/mm^3 and v obtained by (72),(73).

We ran the simulations for 15 h and measured the percentage of cells migrated from the middle chamber. Figure 2 shows the comparison between numerical simulation and experimental data. We observe excellent agreement between simulated and experimental data under static and chemotaxis conditions. The numerical percentage of migrated cells at time $t = 15$ h falls within the laboratory experiments' error bars (mean $\pm$ SD). Under chemotaxis and flow conditions, the numerical result of 3.0% falls outside the experimental error bar (3.3%-3.4%). According to [23], flow alone has a small additional effect on cell migration due to ECM degradation by proteolysis. Our model does not replicate this phenomenon, which may explain the discrepancy between numerical and experimental results.

Under static conditions, the percentage of migrated cells (0.4%) is three times lower than under chemotaxis conditions (1.2%). By adding flow contribution, this value rises above 3.0%.

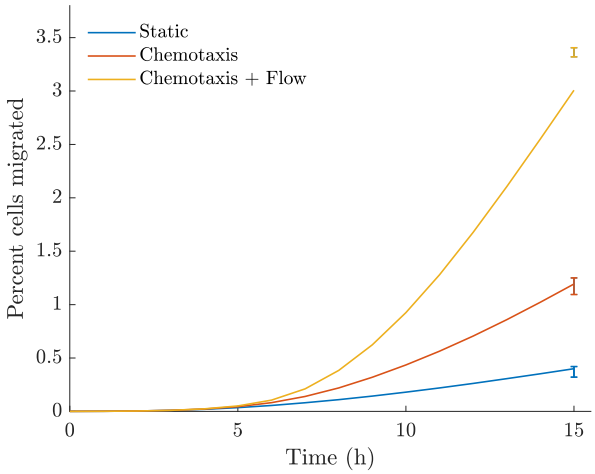

Figure 2: Comparison of experimental and simulated tumor cell migration results. Error bars indicate the mean ± standard deviation of experimental results for MDA-MB-435S tumor cells at $t = 15$ h, as reported in [23]. Experimental data for static and chemotaxis conditions are from Figure 4 in [23], while chemotaxis plus flow data are from Figure 7 in [23]. In the numerical simulations, we used a uniform mesh $h = k = 0.005$ mm and a uniform time step $\Delta t = 1$ h. Mesh sensitivity analysis revealed that the simulations are mesh-independent.

The release of bound CCL21 creates a chemoattractant gradient toward the bottom chamber (Figure 3, top row on the left). The cells sense and react to this gradient, migrating to the bottom chamber (Figure 3, middle row on the left). Adding flow towards the bottom chamber raises the chemoattractant gradient near the bottom chamber (Figure 3, top row on the right), enhancing tumor cell chemotaxis (Figure 3, middle row on the right). The increased bound CCL21 release under flow conditions (Figure 3, bottom row) also reflects the improved cell migration. These results show how chemotaxis and interstitial flow combine for tumor cell migration toward the CCL21-secreting lymphatics. For completeness, we show in Figure 4 the velocity field associated with flow conditions.

5 Conclusions

This paper focuses on a general nonlinear Keller-Segel-Darcy model that combines the classical parabolic Keller-Segel system with the elliptic Darcy equation. We proposed a fully discrete scheme of type IMEX-FDM and established sharp convergence error estimates. Numerical experiments validate these results. The Keller-Segel-Darcy model extends the traditional Keller-Segel by allowing the simulation of relevant chemotaxis phenomena in fluid environments. One such example is tumor cell migration toward the lymphatics. From a simulation perspective, we investigate the roles of interstitial flow and chemotaxis in this cell migration process. A comparison between numerical and experimental results highlights the model's efficacy but identifies potential areas for improvement, such as incorporating the role of the extracellular matrix. We leave more detailed modeling and simulation work for future research.

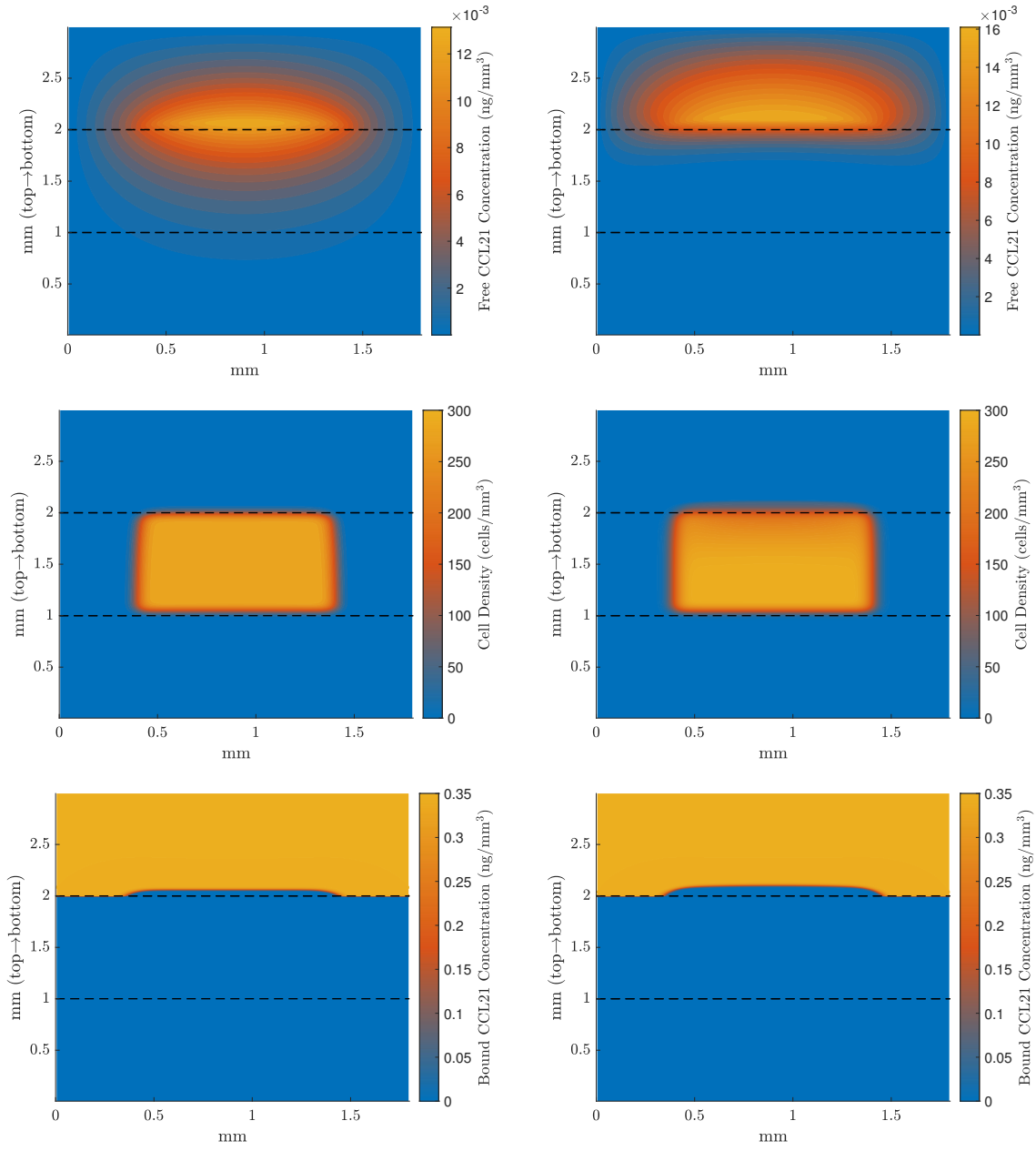

Figure 3: Simulation results of tumor cell migration under chemotaxis (on the left) and chemotaxis plus flow (on the right). From top to bottom: free CCL21 concentration, cell density, and bound CCL21 concentration at time $t = 15$ h.

Acknowledgments

This work was partially supported by the Centre for Mathematics of the University of Coimbra - UIDB/00324/2020, funded by the Portuguese Government through FCT/MCTES. A. Fernandes was also supported by the FCT PhD grant PD/BD/152073/2021, funded by the Portuguese Government through FCT/MCTES.

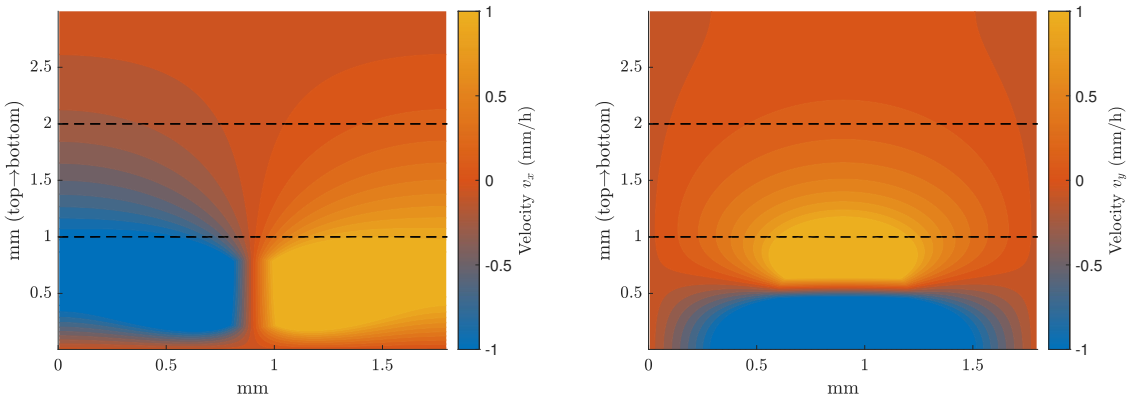

Figure 4: Velocity field $v = (v_x, v_y)$ under flow conditions, v_x on the left and v_y on the right.

References

[1] G. Arumugam and J. Tyagi. Keller-segel chemotaxis models: A review. *Acta Applicandae Mathematicae*, 171(1), 2020.

[2] S. Barbeiro, J. A. Ferreira, and R. D. Grigorieff. Supraconvergence of a finite difference scheme for solutions in $H^s(0, l)$. *IMA Journal of Numerical Analysis*, 25(4):797–811, 2005.

[3] J. Bonilla and J. Vicente Gutiérrez-Santacreu. Exploring numerical blow-up phenomena for the keller-segel-navier-stokes equations. *Journal of Numerical Mathematics*, 32(2), 2023.

[4] G. Chamoun, M. Saad, and R. Talhouk. Numerical analysis of a chemotaxis-swimming bacteria model on a general triangular mesh. *Applied Numerical Mathematics*, 127:324–348, 2018.

[5] M. Chaplain and G. Lolas. Mathematical modelling of cancer invasion of tissue: dynamic heterogeneity. *Networks & Heterogeneous Media*, 1(3):399–439, 2006.

[6] A. Chertock, K. Fellner, A. Kurganov, A. Lorz, and P. A. Markowich. Sinking, merging and stationary plumes in a coupled chemotaxis-fluid model: a high-resolution numerical approach. *Journal of Fluid Mechanics*, 694:155–190, 2012.

[7] C. Chuanmiao and S. Tsimin. *Finite Element Methods for Integrodifferential Equations*. WORLD SCIENTIFIC, Feb. 1998.

[8] Y. Deleuze, C.-Y. Chiang, M. Thiriet, and T. W. Sheu. Numerical study of plume patterns in a chemotaxis-diffusion-convection coupling system. *Computers & Fluids*, 126:58–70, 2016.

[9] A. Duarte-Rodríguez, M. Á. Rodríguez-Bellido, D. A. Rueda-Gómez, and É. J. Villamizar-Roa. Numerical analysis for a chemotaxis-navier-stokes system. *ESAIM: Mathematical Modelling and Numerical Analysis*, 55:S417–S445, 2021.

[10] X. Feng, X. Huang, and K. Wang. Error estimate of unconditionally stable and decoupled linear positivity-preserving fem for the chemotaxis-stokes equations. *SIAM Journal on Numerical Analysis*, 59(6):3052–3076, 2021.

[11] J. Ferreira, H. Gómez, and L. Pinto. A mathematical model for nir light protocol optimization in controlled transdermal drug delivery. *Applied Mathematical Modelling*, 112:1–17, 2022.

[12] J. Ferreira, H. Gómez, and L. Pinto. A numerical scheme for a partial differential system motivated by light-triggered drug delivery. *Applied Numerical Mathematics*, 184:101–120, 2023.

[13] J. A. Ferreira and R. D. Grigorieff. Supraconvergence and supercloseness of a scheme for elliptic equations on nonuniform grids. *Numerical Functional Analysis and Optimization*, 27(5-6):539–564, 2006.

[14] F. Filbet. A finite volume scheme for the patlak-keller-segel chemotaxis model. *Numerische Mathematik*, 104(4):457–488, 2006.

[15] R. Förster, A. C. Davalos-Misslitz, and A. Rot. Ccr7 and its ligands: balancing immunity and tolerance. *Nature Reviews Immunology*, 8(5):362–371, May 2008.

[16] I. Lampropoulos and M. Kavousanakis. Application of combination chemotherapy in two dimensional tumor growth model with heterogeneous vasculature. *Chemical Engineering Science*, 280:118965, 2023.

[17] H. G. Lee and J. Kim. Numerical investigation of falling bacterial plumes caused by bioconvection in a three-dimensional chamber. *European Journal of Mechanics - B/Fluids*, 52:120–130, 2015.

[18] J. C. López-Marcos and J. M. Sanz-Serna. Stability and convergence in numerical analysis III: Linear investigation of nonlinear stability. *IMA Journal of Numerical Analysis*, 8(1):71–84, 1988.

[19] D. O. Miteva, J. M. Rutkowski, J. B. Dixon, W. Kilarski, J. D. Shields, and M. A. Swartz. Transmural flow modulates cell and fluid transport functions of lymphatic endothelium. *Circulation Research*, 106(5):920–931, Mar. 2010.

[20] T. Ortega and J. Sanz-Serna. Nonlinear stability and convergence of finite-difference methods for the "good" boussineq equation. *Numerische Mathematik*, 58:215–229, 1990.

[21] M. Pisano, V. Triacca, K. A. Barbee, and M. A. Swartz. An in vitro model of the tumor-lymphatic microenvironment with simultaneous transendothelial and luminal flows reveals mechanisms of flow enhanced invasion. *Integrative Biology*, 7(5):525–533, 2015.

[22] G. S. Rosalem, E. B. Las Casas, T. P. Lima, and L. A. González-Torres. A mechanobiological model to study upstream cell migration guided by tensotaxis. *Biomechanics and Modeling in Mechanobiology*, 19(5):1537–1549, 2020.

[23] J. D. Shields, M. E. Fleury, C. Yong, A. A. Tomei, G. J. Randolph, and M. A. Swartz. Autologous chemotaxis as a mechanism of tumor cell homing to lymphatics via interstitial flow and autocrine CCR7 signaling. *Cancer Cell*, 11(6):526–538, June 2007.

[24] J. D. Shields, I. C. Kourtis, A. A. Tomei, J. M. Roberts, and M. A. Swartz. Induction of lymphoidlike stroma and immune escape by tumors that express the chemokine ccl21. *Science*, 328(5979):749–752, May 2010.

[25] Y. Tang, G.-a. Zou, and J. Li. Unconditionally energy-stable finite element scheme for the chemotaxis-fluid system. *Journal of Scientific Computing*, 95(1), 2023.

[26] J. O. Waldeland and S. Evje. A multiphase model for exploring tumor cell migration driven by autologous chemotaxis. *Chemical Engineering Science*, 191:268–287, Dec. 2018.

[27] J. O. Waldeland, J.-V. Gaustad, E. K. Rofstad, and S. Evje. In silico investigations of intratumoral heterogeneous interstitial fluid pressure. *Journal of Theoretical Biology*, 526:110787, Oct. 2021.

[28] M. Wang, G.-a. Zou, B. Wang, and W. Zhao. Unconditionally energy-stable discontinuous galerkin method for the chemo-repulsion-navier-stokes system. *Computers & Mathematics with Applications*, 150:132–155, 2023.

[29] M. A. Winkelman, D. Y. Kim, S. Kakarla, A. Grath, N. Silvia, and G. Dai. Interstitial flow enhances the formation, connectivity, and function of 3d brain microvascular networks generated within a microfluidic device. *Lab on a Chip*, 22(1):170–192, 2022.